ELSEVIER

Journal of Volcanology and Geothermal Research 63 (1994) 267–279

Journal of volcanology and geothermal research

Interactions between bubbles in magmas and lavas: effects of bubble deformation

Michael Manga[a], H.A. Stone[b]

[a]*Department of Earth and Planetary Sciences, Harvard University, Cambridge, MA 02138, USA*
[b]*Division of Applied Sciences, Harvard University, Cambridge, MA 02138, USA*

Received 16 November 1993; accepted 1 April 1994

Abstract

The interactions between two deformable bubbles are studied in order to determine the effects of deformation on bubble dynamics and to determine the limits in which the effects of deformation can be ignored. Deformation due to hydrodynamic interactions with other bubbles leads to alignment of horizontally offset bubbles and thus an enhanced rate of coalescence. Bubble alignment may produce spatial inhomogeneities in bubble concentrations in magmas, which implies temporal variations in the concentration and size of bubbles in erupting magmas and spatial variations in solidified lavas. An approximate quantitative model for the rate of coalescence of deformable bubbles is developed based on a series of experiments. The effects of deformation can be ignored if the largest bubbles have radii less than about 5 mm in silicate magmas.

1. Introduction

The dynamics of bubbles in magmas affect volcanic processes and the behaviour of related magmatic systems. For example, the interactions and coalescence of bubbles in ascending magmas and magma chambers may be important processes governing the style of volcanic eruptions (e.g., Wilson and Head, 1981; Jaupart and Vergniolle, 1988). Bubble coalescence is also inferred to occur frequently in basaltic flows (e.g., Sahagian et al., 1989; Walker, 1989; Herd and Pinkerton, 1993), thus affecting the spatial and size distribution of bubbles in solidified lavas. The rate of coalescence and ascent of bubbles in molten rock is also of interest during the process of in situ vitrification, which is a treatment method for contaminated soils. The contaminated region is melted and later allowed to resolidify; organic and volatile components in the soil are pyrolyzed and vapourized, respectively, and the gases rise in the form of bubbles to the surface of the molten region where combustion occurs (Jacobs et al., 1988).

Owing to the large viscosities of silicate magmas, which range from 30 Pa s for some basalts to 10^7 Pa s for some rhyolites (Bottinga and Weill, 1972), bubble dynamics in magmas are typically characterized by small Reynolds numbers:

$$Re=\frac{\rho U a}{\mu}<1 \qquad (1)$$

where μ is the magma viscosity, ρ is the magma density, a is the bubble radius, and U is the bubble rise speed. Bubbles are predicted to reach diameters of 0.1 to 5 cm in basalts due to growth by diffusion and depressurization as they rise

SSDI 0377-0273(94)00031-B

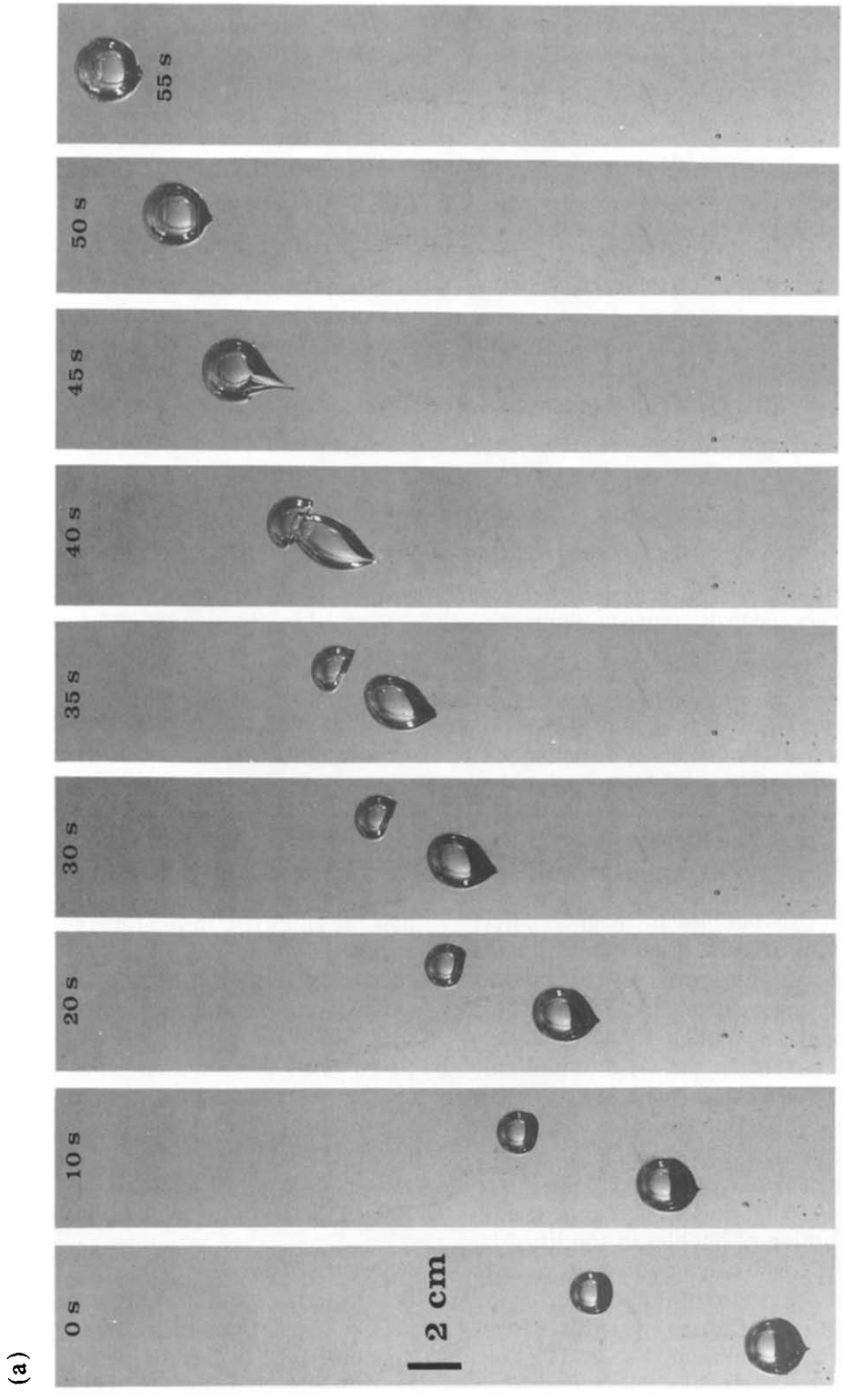
0 s
10 s
20 s
30 s
35 s
40 s
45 s
50 s
55 s
2 cm
(a)

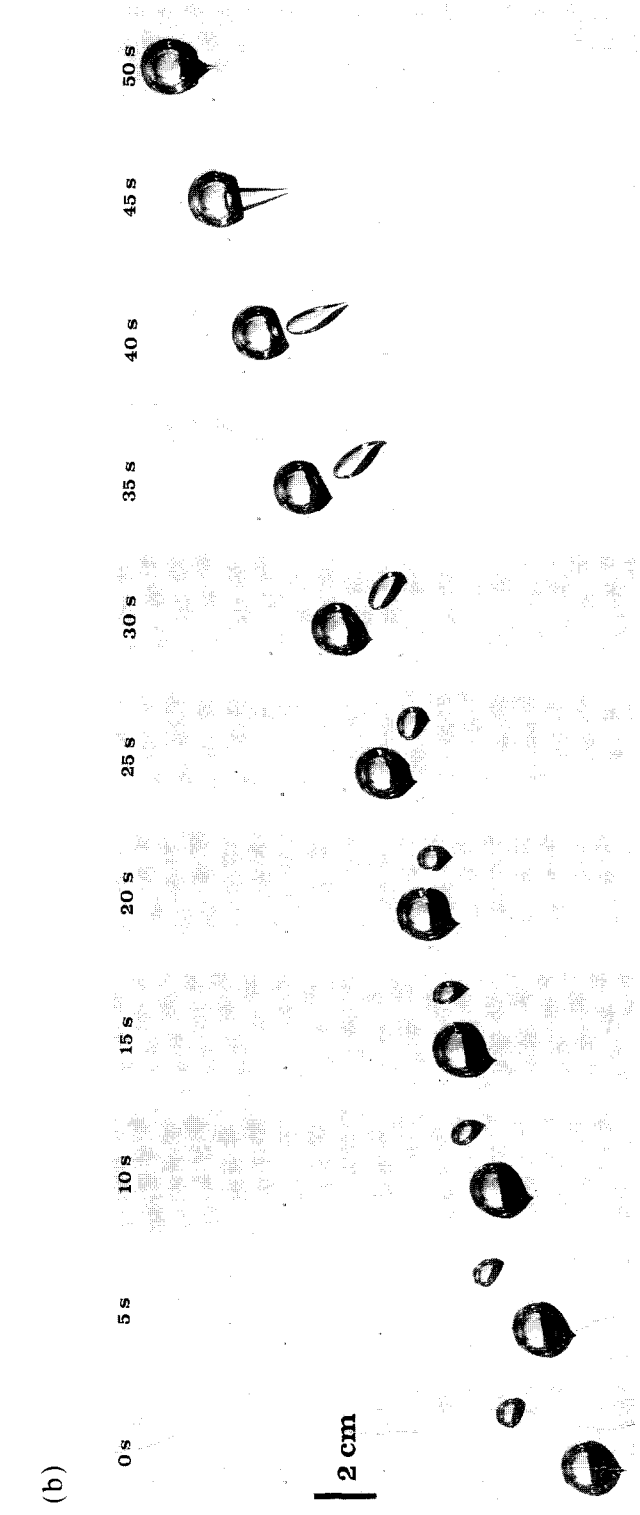

Fig. 1. Interaction and deformation of two air bubbles rising in a large container of corn syrup: (a) alignment and (b) 'suction' or entrainment of bubbles which are initially horizontally offset. The Reynolds number (Re) ≈ 0.005, and the Bond number (B) ≈ 20. Photographs are taken at 5-s intervals. The trailing bubble initially has a small tail; the tail develops as the bubble is formed and, owing to the large viscosity of the corn syrup, does not relax before the first photograph is taken. Coalescence occurs between the last two photographs shown in (a) and shortly after the last photograph shown in (b).

(Sparks, 1978; Proussevitch et al., 1993a), although the observed size of bubbles preserved in basalts is often less than 1 cm (Sarda and Graham, 1990; Mangan et al., 1993). The degree of deformation is governed by the Bond number:

$$B=\frac{\Delta\rho g a^2}{\sigma} \quad (2)$$

which represents the ratio of buoyancy forces relative to the surface tension forces that resist deformation (σ is the surface tension and g is gravitational acceleration, and $\Delta\rho$ is the density difference between the magma and gas in the bubble). The surface tension between silicate magmas and gases at atmospheric pressure is 0.35–0.37 N/m (Walker and Mullins, 1981), thus for bubbles with radii of 1 cm, $B\approx 10$. At higher pressures, the surface tension between water vapour and melts may be significantly reduced, with a magnitude about 0.1 N/m at pressures of 300 MPa (Khitarov et al., 1979).

We show below that for $Re \ll 1$ and $B > O(1)$ bubble interactions lead to significant shape distortions, which affect the translation, coalescence and spatial distribution of bubbles. Bubble deformation and coalescence will be important processes provided sufficient time exists for bubble interactions to influence coalescence, as expected in magma chambers (Vergniolle and Jaupart, 1986, 1990) and during eruptions with slow ascent rates (Toramoru, 1988). Interactions and coalescence should also affect the resulting distribution of bubbles in cooling and solidifying magmas (Sahagian, 1985; Sahagian et al., 1989).

2. Two-bubble interactions

Owing to the complexity of bubble dynamics and coalescence, bubble hydrodynamics are generally ignored or parameterized in studies of eruption processes (Wilson and Head, 1981; Vergniolle and Jaupart, 1986), bubble migration in cooling lavas (Sahagian, 1985; Sahagian et al., 1989), and studies interpreting bubble size distributions (Toramoru, 1990; Sarda and Graham, 1990). In this paper we consider the dynamics associated with the buoyancy-driven translation and deformation of a pair of bubbles. As with many multiphase systems, characterization of two-particle interactions provides a useful model for understanding the behaviour of systems with many bubbles. The dynamics considered here should be applicable to bubbles in magmas provided the concentration of bubbles is low enough that the bubbles are able to rise and interact although the quantitative details of many-bubble systems may differ from two-bubble interactions. At bubble concentrations greater than 74%, when all the bubbles are in near contact, the system is best described as a foam and will have different dynamics (Proussevitch et al., 1993b).

2.1. Alignment and entrainment of offset bubbles

In order to simulate bubble interactions in basaltic magmas, we performed simple experiments with bubbles in a large container of corn syrup. In Fig. 1 we show two sequences of photographs highlighting the role of deformation for $B\approx 20$ and $Re\approx 5\times 10^{-3}$, parameters scaled to bubbles with radii of about 1 cm in silicate magmas. The experiment in Fig. 1a illustrates bubble alignment for two horizontally offset bubbles in which the leading bubble coats the trailing bubble. In Fig. 1b the small bubble is advected around the larger bubble and is 'sucked' or entrained into the rear of the larger bubble. Coalescence occurs shortly after the time of the last photograph shown in Fig. 1a and between the last two photographs shown in Fig. 1b. For each of the interactions shown in Fig. 1 we note the large degree and complexity of deformation of both bubbles and the formation of tails and regions of high curvature. Although the process of bubble coalescence is complicated and difficult to parameterize for highly deformed bubbles, the behaviour of bubbles in magmas and lavas can be scaled to the results presented in Fig. 1 because the Bond number and Reynolds numbers are similar to those in magmas and lavas; only the time scale for the interaction to occur will change, scaling as $\mu/\rho g a$.

The importance of deformation is apparent

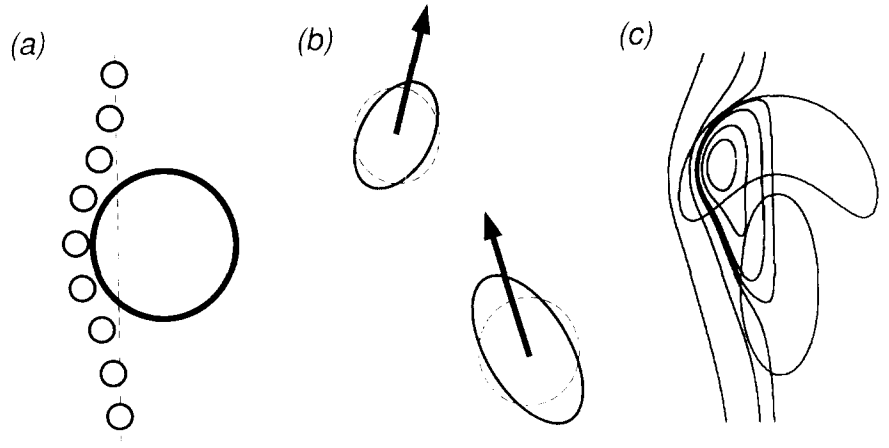

Fig. 2. (a) Illustration of the interaction of spherical bubbles. Relative to the larger bubble, the small bubble is swept around the larger bubble. (b) Illustration of the process of bubble alignment: undeformed shapes are shown with dashed lines and deformed shapes are shown with solid lines. The stress field produced by each bubble deforms the other bubble leading to a horizontal component of translation which tends to align the bubbles. (c) Calculated streamlines for a pair of translating and deforming axisymmetric drops. The streamlines are shown in a frame of reference translating with the front of the larger drop. The figure shows the formation of a 'wake' (due to deformation) which leads to entrainment. The time-dependent deformation and the streamlines are calculated using a boundary integral method (Manga and Stone, 1993). The drops have the same viscosity as the surrounding fluid; $B=50$.

when we note that the corresponding low Reynolds number flow problem of two translating spherical (i.e. undeformed) bubbles evolves so that, relative to a reference frame translating with the larger bubble, the small bubble is swept around the larger bubble and the bubbles do not coalesce (Fig. 2a). The off-axis configuration of two bubbles is unstable as a consequence of the hyperbolic stagnation point at the front of the larger bubble.

A qualitative explanation for the alignment of deformable offset bubbles (Fig. 1a) is illustrated schematically in Fig. 2b. Alignment occurs since the effect of bubble interactions is to deform the trailing bubble into a prolate shape, suitably inclined with respect to the vertical; the leading bubble is deformed into an oblate shape. The inclined shapes lead to small horizontal components of translation which tend to align the bubbles. Thus, even equal-sized deformable bubbles interact in a manner leading to eventual coalescence.

The second type of two bubble interaction (Fig. 1b), in which the small bubble is first advected around the larger bubble and then sucked in from behind, arises due to the deformation of the larger bubble. The entrainment dynamics result from the continual deformation of the larger bubble so that in a frame of reference moving with the larger bubble, streamlines intersect the interface and a vortex or wake is generated behind the bubble (even at zero Reynolds numbers). To illustrate this mode of interaction, we show in Fig. 2c numerically computed streamlines for a pair of translating drops which have the same viscosity as the surrounding fluid and $B=50$ (Manga and Stone, 1993). The continual deformation at the back of the leading drop results in closed streamlines which leave and reenter the drop defining a vortex which may entrain a trailing drop. At higher Reynolds numbers alignment may also occur for two spherical bubbles owing to the formation of a low pressure wake (De Nevers and Wu, 1971).

2.2. The rate of coalescence of deformable bubbles

The complexity of the interaction of deformable bubbles prohibits the use of analytical results

and numerical studies (e.g., Manga and Stone, 1993) to quantitatively characterize the interaction of deformable bubbles. Thus, we performed a large number of experiments characterizing the interaction of air bubbles in corn syrup in order to develop a model for the coalescence of bubbles in magmas. In the experimental results presented here we consider only the limit in which large distortions occur so that the deformation, as observed in Fig. 1, results in the capture and coalescence of bubbles. Interfacial effects such as Van der Waals forces or the presence of surfactants are important for the eventual coalescence of two bubbles; however, for the limit of large distortions considered here, such effects will only play a minor role in the rate of coagulation of bubbles. The experiments were performed in a large tank, with dimensions $61 \times 61 \times 122$ cm, filled with corn syrup (Fig. 3). Bubbles were injected into the bottom of the tank through a sequence of regularly spaced holes fitted with one-way valves. Bubble volume was measured by calibrating a series of syringes. The error in measuring bubble volume was always less than 5%. In the experiments, a smaller bubble was injected first. In order to minimize the effects of not having an initially infinite vertical separation distance between the bubbles, the second larger bubble was injected once the small bubble has risen at least 25 cm. In order to minimize boundary effects, all interactions were required to occur at least 25 cm away from a boundary (side walls, the upper free-surface and the lower rigid boundary) in order to be included as acceptable data.

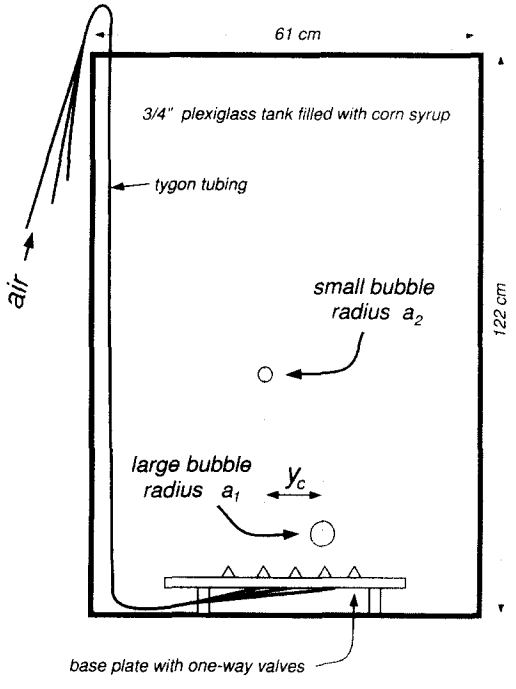

Fig. 3. Schematic diagram of the tank used for the experiments presented in Figs. 4 and 5. The tank is made of $^3/_4$" plexiglass. Bubbles are injected into the tank from calibrated syringes connected to tygon tubing and one-way valves. The radii of the larger and smaller bubbles are a_1 and a_2, respectively, and the horizontal separation distance between the bubbles which separates interactions in which coalescence occurs from trajectories in which the bubbles to not coalesce is y_c.

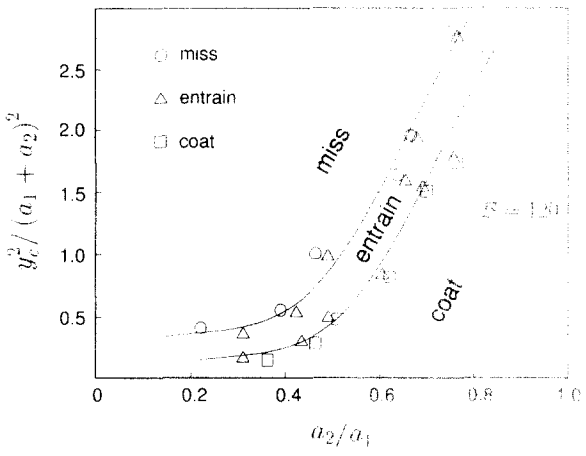

Fig. 4. The mode of bubble interaction as a function of bubble offset, y_c, and relative bubble size, a_2/a_1, for $B=120$. 'Coat' refers to interactions as in Fig. 1a (□), 'entrain' refers to interactions as in Fig. 1b (△), and 'miss' refers to interactions in which the bubbles do not coalesce (○). The bubbles are initially separated vertically by at least $10a_1$.

In Fig. 4, we present a series of experimental results which separate the three different possible modes of bubble interactions for $B=120$. For convenience we assume that the radius of the larger bubble is a_1 and the Bond number is based on the radius of the larger bubble, $B=\Delta\rho g a_1^2/\sigma$. The data illustrate that for a given horizontal separation distance, y, coalescence is more likely if the bubbles have a nearly equal size than a very

large size difference. For a given relative size (fixed a_2/a_1, see Fig. 3), as the separation distance is increased: (1) the bubbles first interact such that the smaller bubble spreads over or 'coats' the larger bubble (as in Fig. 1a); (2) as the horizontal separation distance is gradually increased, the small bubble may be advected around the larger bubble and then entrained inside the larger bubble (as in Fig. 1b); and finally (3) for still greater horizontal separation distances, the small bubble is advected around the larger bubble and coalescence does not occur.

In order to calculate the evolution of the bubble size distribution, the interaction between two bubbles is generally used as a model for the interactions occurring in a suspension, an approximation rigorously valid only for dilute suspensions. Specifically, the rate of coalescence of bubbles of radius a_1 with bubbles of radius a_2 is given by (e.g., Davis, 1984):

$$J_{12} \approx n_1 n_2 \pi (U_1 - U_2) y_c^2 \left(B, \frac{a_2}{a_1} \right) \tag{3}$$

where n_i is the number of bubbles of radius a_i per unit volume, $(U_1 - U_2)$ is the difference in the rise speeds of the bubbles, and y_c (which can be interpreted as a capture radius) is the horizontal separation distance for large vertical separation distances which separates bubble trajectories which result in coalescence and trajectories of bubbles which miss each other (see Fig. 3). The rise speed U of an isolated bubble at low Reynolds number is given by:

$$U = \frac{\Delta \rho g a^2}{3\mu} \tag{4}$$

In Fig. 5 we present experimental measurements of the capture radius y_c in Eq. (3) as a function of B and the relative bubble radius a_2/a_1; we use these results to construct an approximate quantitative model for bubble coalescence. Results are presented for $B = 15$, 30, 73 and 120. Data points represent interactions which result in coalescence (such as in Fig. 1) and interactions in which no coalescence occurs. Error bars are not shown. Typical errors on measurements of bubble radii are always less than about 2%.

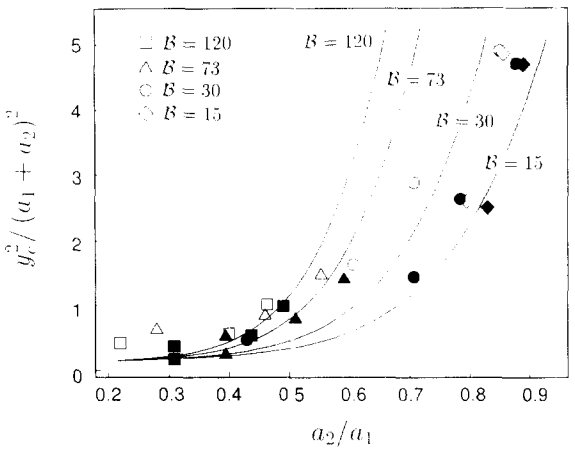

Fig. 5. Experimental results used to derive an approximate quantitative model for the coalescence of deformable bubbles. Acceptable experimental results require that the initial condition is a good approximation to bubbles with an infinite vertical separation (see discussion in the text). Results are presented for $B = 120$ (□), $B = 73$ (△), $B = 30$ (○) and $B = 15$ (◇). Open symbols represent interactions in which the bubbles do not coalesce; filled symbols represent interactions in which the bubbles coalesce. Error bars are not shown. The solid curves represent predictions of a model described by Eq. (5).

Data presented in Fig. 5 are deemed acceptable if the initial vertical separation distance is sufficiently large; specifically, we require that the magnitude of bubble distortion due to bubble interaction for the initial separation distance was less than 10% (as predicted by Manga and Stone, 1993). Despite the large volume of the tank, we could only accept experimental results for a limited number of horizontal bubble separation distances, Bond numbers and relative bubble sizes. A larger apparatus would be necessary to collect additional data for bubbles with large Bond numbers ($B = 73$ and 120). For comparison, predictions from a model of the form:

$$\frac{y_c^2}{(a_1 + a_2)^2} = 0.3 \left(\frac{a_2}{a_1} \right)^{1/2} + \frac{1}{2} B \left(\frac{a_2}{a_1} \right)^6 \tag{5}$$

are shown with solid lines for the four values of the Bond numbers corresponding to the experimental measurements. From Eq. (5), in the limit that $B \to 0$ we approximately recover the result of Zhang and Davis (1991) for spherical bubbles. Equation (5) is *not* based on analytical results or

theory, but is only a useful functional relationship between the capture cross section y_c^2, the Bond number, and the relative bubble size which is approximately consistent with the limited amount of experimental data.

We note that the capture cross section may even be larger than the sum of the bubble radii (as illustrated in Fig. 1). A capture cross section equal to the sum of the bubble radii, $y_c^2/(a_1+a_2)^2=1$, corresponds to the interaction between spherical bubbles moving vertically with no hydrodynamic interactions (so that smaller bubbles are not advected around larger bubbles).

The dimensionless rate of coalescence, J_{12}, is shown in Fig. 6 for the model described by Eq. (3) and a capture cross section defined by Eq. (5). The rate of coalescence of deformable bubbles is often more than one order of magnitude greater than for spherical bubbles for a wide range of size ratios, e.g., $0.7<a_2/a_1<1$ when $B=10$. For small a_2/a_1, the effects of deformation are small, although the magnitude of deformation may be large, and small bubbles tend to follow streamlines and are advected around larger bubbles. As $a_2/a_1\to 1$, Eq. (5) predicts no coalescence since the relative velocity of the bubbles $U_1-U_2\to 0$. However, as discussed in Manga and Stone (1993), shape changes due to deformation will result in the eventual coalescence of equal-sized bubbles. Thus, the model described by Eqs. (3)–(5) underestimates the rate of coalescence as $a_2/a_1\to 1$.

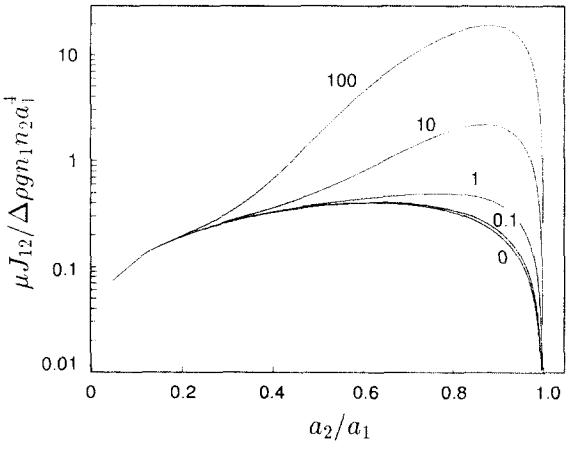

Fig. 6. Dimensionless rate of coalescence based on the model described by Eqs. (3–5) for $B=0$, 1, 10 and 100. We emphasize that the model is *not* based on analytical results or theory, but is only a useful functional relationship between the capture cross section, y_c^2, the Bond number, and the relative bubble size which is approximately consistent with the limited amount of experimental data presented in Fig. 5.

3. Applications to bubbles in magmas and lavas

Below we consider some volcanological problems involving basaltic magmas and lavas in which bubble interactions may occur. The processes illustrated in Fig. 1 may not be the dominant processes governing the style of basaltic eruptions and the behaviour of bubbles in lavas; nevertheless, the two bubble coalescence experiments highlight some of the consequences of bubble interactions which will occur between the larger bubbles in magmas (radii greater than about 0.5 cm), and may play a previously unrecognized role in the dynamics of volcanic and magmatic systems. In the experimental results shown in Fig. 1, bubbles typically interact and deform over a translational distance of a few bubble diameters: in some volcanic systems, magma chambers and lava flows, magma velocities are sufficiently small that time will exist for interactions and coalescence of bubbles to occur.

3.1. The formation of instabilities of bubble concentration

The alignment and coalescence of bubbles may give rise to spatial inhomogeneities of bubble concentrations which lead to temporal variations in the amount of gases erupted with magmas. Bubble migration due to the deformed bubble shapes (Fig. 2b) may lead to spatial inhomogeneities analogous to those which develop in suspensions of ellipsoidal particles (Koch and Shaqfeh, 1989); for example, in an initially homogeneous and monodisperse suspension of bubble the length scale of the instability:

$$\lambda\approx\frac{1}{\sqrt{na}} \qquad (6)$$

where n is the number of bubbles per unit volume and a is the radius of the bubbles. The instability arises since variations of bubble concentration will lead to velocity gradients in the magma which deform bubbles. Deformed bubbles will migrate from a region of low to high bubble concentration, as schematically illustrated in Fig. 7. The growth rate of the instability will depend on the magnitude of bubble deformation and thus on the Bond number, and therefore we expect that the larger bubbles in a magma will set the length scale of the instability. In a magma with a volume fraction of 0.1% vesicles with radius 1 cm, the length scale of the instability will be on the order of half a meter and might be observed in solidified lavas.

We also note that, based on the study of Koch and Shaqfeh (1989), spatial inhomogeneities in the concentration of sedimenting olivine crystals will develop. The occurrence of aggregates of olivine crystals in some Hawaiian basalts (Schwindinger and Anderson, 1989) may arise from such an instability.

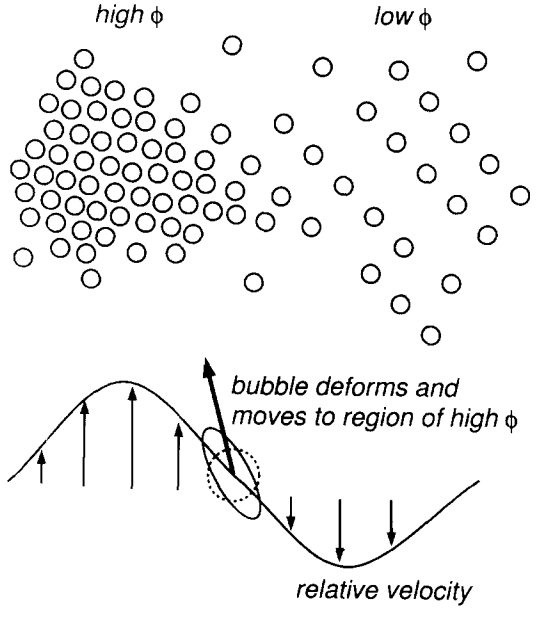

Fig. 7. Schematic illustration of the development of spatial variations of bubble concentration (after Koch and Shaqfeh, 1989). Variations of bubble concentration lead to variations of bubble rise speeds and thus local velocity gradients. Velocity gradients deform bubbles which wilt then migrate from a region of lower to higher bubble concentration.

3.2. Applications to volcanic systems

Spatial variations of bubble concentration have been proposed to explain the temporal variations in eruptive style in Kilauea (Jaupart and Vergniolle, 1990), with periods of high gas flow resulting in fire fountaining, whereas magmas with low bubble concentrations are extruded smoothly. If sufficient bubble coalescence occurs, a conduit filling gas plug or cluster of bubbles may develop resulting in strombolian eruptions (Blackburn et al., 1976). Previous calculations suggest that for magma rise speeds in the conduit $U_{\text{magma}} > 1$ m/s fire fountaining will occur, whereas for $U_{\text{magma}} < 0.1$ m/s sufficient time exists for coalescence to produce conduit-filling gas plugs which result in discrete strombolian eruptions (Wilson and Head, 1981). Image processing of eruptions at Stromboli suggests that individual eruptions consist of single impulses (thus, a single large bubble) and more frequently successive pulses with time intervals of about 1 s (thus, a sequence of closely spaced bubbles) (Ripepe et al., 1993).

The long duration of fire-fountaining events, typically one day, is greater than the residence time of the magma in the rift zone which is typically a few hours (Wilson and Head, 1981). The models by Jaupart and Vergniolle (1988, 1990) thus require that bubble accumulation and coalescence occurs at the top of a magma chamber in order to account for the extended duration of fire fountaining. However, degassing at Kilauea is thought to be a two-stage process, with gases in the magma chamber vented through fumaroles, whereas carbon-depleted gases, which form at depths less than a few hundred meters, are vented through eruptions in the rift zones (Greenland et al., 1985; Gerlach and Graeber, 1985). We note that the enhancement of bubble coalescence by bubble alignment is an additional mechanism which may allow spatial variations in bubble concentrations to develop in the magma chamber (as well as in the conduit) without necessarily involving the accumulation of a bubbly or

foam layer at the top of a magma chamber.

The physics of bubble interactions shown in Fig. 1 is relevant to the interaction between clouds of bubbles (discrete regions in the magma with a much larger bubble concentration than the surrounding magma characterized by very large Bond numbers) which may form following the breakup of the foam at the roof of a magma chamber (Jaupart and Vergniolle, 1988). The interactions of bubbles and bubble clouds in the magma chamber or conduit may help account for the significant variations of eruption heights (fountain heights vary from 10 to 400 m) which change over periods of a few hours (Head and Wilson, 1987). The final coalescence of bubbles into larger bubbles may involve the coalescence of bubbles in a foam rather than by the processes illustrated in Fig. 1 depending on the concentration and size of the bubbles.

We note that the bubbles preserved in lavas and contained in effusive magmas may not be representative of those in erupting magmas. The largest bubbles responsible for fire fountaining and explosive events will be destroyed during eruption — small bubbles (i.e. small Bond numbers, hence, small deformations) are swept around larger bubbles (Fig. 2a) and will generally still be present in the effusive volcanic lavas.

3.3. Application to bubbles in lava flows

Bubble coalescence is thought to be an important process causing changes of bubble-size distribution in some quiescent lava flows (McMillan et al., 1987; Sahagian et al., 1989) and flowing lavas (Walker, 1989). In systems containing very small bubbles (thus small Bond numbers) such as the mid-ocean ridge basalts studied by Sarda and Graham (1990) and the Kilauean basalts studied by Mangan et al. (1993) coalescence is inferred to not occur frequently. The final distribution of bubbles in solidified lavas may be used to infer atmospheric pressure at the time the lavas were erupted and thus may be used to infer paleobathymetry, paleoelevation, and uplift or subsidence histories (Sahagian et al., 1989).

An example of a lava flow in which bubbles may have large Bond numbers and bubble coalescence was probably an important process governing the final size distribution of bubbles is the Cohassett flow of the Grande Ronde Basalt (McMillan et al., 1987). The flow is typically 70 m thick and contains two distinct layers with high vesicularities, an upper layer near the top of the flow, and an internal vesicular layer about 4 m thick at a depth of about 40% of the flow thickness, see Fig. 8 which has been adapted from McMillan et al. (1987). The flow-top vesicular region forms soon after the emplacement of the flow and consists of bubbles initially contained in the erupted magma. The internal vesicular

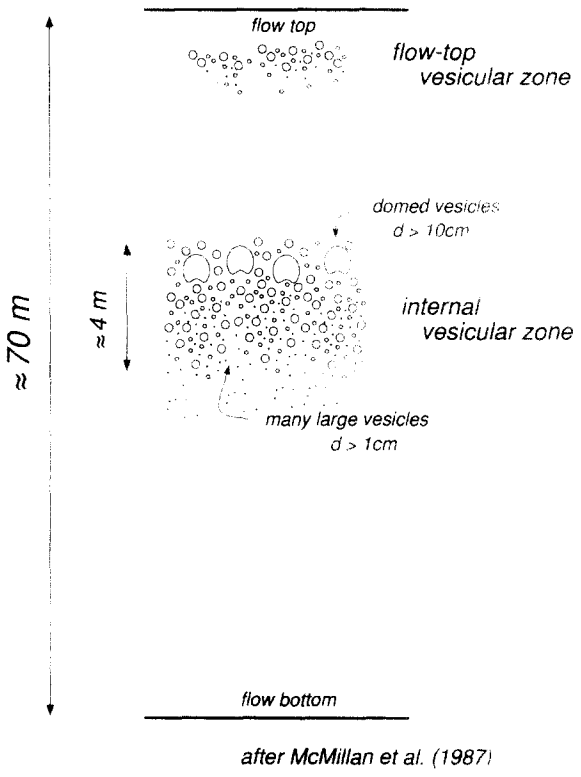

Fig. 8. Schematic cross section of the Cohassett flow of the Columbia River basalts (after McMillan et al., 1987, fig. 2). The flow-top vesicular region forms shortly after the emplacement of the flow and consists of bubbles initially contained in the erupted magma. McMillan et al. (1987) proposed that the internal vesicular zone consists of bubbles nucleated at the lower solidification front which have risen and coalesced to create a number of large vesicles, with diameters d greater than 1 cm, and very large domed vesicles with d greater than 10 cm.

zone contains bubbles nucleated at the lower solidification front which have risen and coalesced to create a number of large vesicles, with diameters d greater than 1 cm, and very large domed vesicles with d greater than 10 cm. Lava flows with thickness less than 10 m show no internal vesicular zone and little evidence for coalescence except for the presence of a small number of vesicles with radii a greater than 1 cm (Aubele et al., 1989).

Larger bubbles formed as a result of coalescence rise and separate more rapidly (Wilson and Head, 1981) resulting in spatial variations of bubble size and concentration thus producing the observed gradation of bubbles sizes in the internal vesicular zone, with larger bubbles near the top and smaller bubbles near the bottom. The calculations of Sahagian (1985) demonstrate the separation of bubble sizes due to differential ascent rates. However, the quantitative details of the bubble distribution in solidified lavas may differ from the predictions of Sahagian owing to the effects of deformation, which will result in a rate of coalescence greater for deformable bubbles ($a > 5$ mm) than for spherical bubbles, as demonstrated in Fig. 6.

Many lava flows contain vertically aligned structures called pipe vesicles and vesicle cylinders (e.g., Goff, 1977; Walker, 1987; Aubele et al., 1989; Sahagian et al., 1989). We make the distinction, following Philpotts and Lewis (1987), between pipe vesicles which are elongated tubes with typical diameters of 5 mm and lengths greater than 10 cm and vesicle cylinders which are composed of highly vesicular basalt with typical diameters of several centimeters, lengths up to several meters, and often regular spacing between cylinders with separations of tens of centimeters (Goff, 1977). Vesicles cylinders commonly contain large vesicles with radii greater than a few millimeters and are generally located in the interior of a flow (Goff, 1977; Aubele et al., 1989). The coalescence of pipes vesicles observed by Walker (1987) may be due to the mechanisms of coalescence discussed in this paper if the bubbles rise due to buoyancy forces. Goff (1977) proposes that vesicle cylinders form as a result of a Rayleigh–Taylor instability of a highly vesicular layer in basalts with high concentrations of dissolved water. The instability discussed in Section 3.1 may be an additional mechanism leading to the formation of vesicles cylinders; further experimental and analytical work is necessary to predict the implications of bubble alignment on the formation of vesicular structures in lava flows.

4. Concluding remarks

In this paper we have considered an experimental model for the interaction of bubbles in magmas and lavas; the results presented here are strictly applicable only for sufficiently dilute systems of bubbles in magmas that buoyancy-driven interactions occur. Numerical and analytical calculations demonstrate that the inclined ellipsoidal shapes (Fig. 2b) lead to horizontal components of translation which tend to align even widely separated bubbles (Manga and Stone, 1993). A simple consequence of bubble interactions is that the capture cross section for coalescence of comparable-sized bubbles may much larger than the sum of the bubble radii. Previous investigations have assumed a capture cross section proportional to the square of the radius of the smaller bubble (Wilson and Head, 1981) or have ignored the important hydrodynamic effects associated with deformation (Sahagian, 1985; Sahagian et al., 1989). For sufficiently deformable bubbles, $B > O(1)$, and bubbles with comparable sizes, the effects of deformation will promote the coalescence of bubbles — thus, the physics of deformable bubbles and consequences of deformation for multiple bubble interactions at low Reynolds numbers are fundamentally different from spherical bubbles. The experimental results presented in Section 2 demonstrate that results which neglect the effects of deformation underestimate the rate of coalescence of bubbles, perhaps by more than an order of magnitude in a system with a greater than 0.5 cm. The effects of deformation can be neglected if the largest bubbles have Bond numbers less than $O(1)$, which corresponds to bubbles with radii less than a few millimeters in silicate magmas.

The enhancement of coalescence of bubbles will have a few possibly important effects: (1) larger bubbles will form and rise quickly resulting in the separation of larger bubbles from smaller bubbles (the rise speed in Stokes flow is proportional to the square of the radius); (2) the ratio of surface area to volume decreases as bubble size increases, so that the total surface area over which reactions, diffusion and absorption of various chemical species can occur decreases as coalescence occurs; (3) an instability may occur such that spatial variations of bubble concentration develop. We expect that a better understanding of bubble dynamics in magmas combined with measurements of bubble size distributions may provide additional constraints on the depth of bubble nucleation, bubble growth rates, and magma dynamics in conduits and magma chambers.

Acknowledgements

This work was supported by I.G.P.P. grant 351 from Los Alamos National Lab, the American Chemical Society, and NSF grants CTS8957043 and EAR9218923. Reviews by Kathleen Schwindinger and Dork Sahagian have greatly improved this paper. We thank Harvard undergraduate Joe Rice for assistance with the experiments.

References

Aubele, J.C., Crumpler, L.S. and Elston, W.E., 1989. Vesicle zonation and vertical structure of basalt flows. J. Volcanol. Geotherm. Res., 35: 349–374.

Blackburn, E.A., Wilson, L. and Sparks, R.S.J., 1976. Mechanisms and dynamics of Strombolian activity. J. Geol. Soc. London, 132: 429–440.

Bottinga, Y. and Weill, D.F., 1972. The viscosity of magmatic silicate liquids: A model for calculation. Am. J. Sci., 272: 438–475.

Davis, R.H., 1984. The rate of coagulation of a dilute polydisperse system of sedimenting spheres. J. Fluid. Mech., 145: 179–199.

De Nevers, N. and Wu, J.-L., 1971. Bubble coalescence in viscous fluids. AIChE J., 17: 182–186.

Gerlach, T.M. and Graeber, E.J., 1985. Volatile budget of Kilauea volcano. Nature, 313: 273–277.

Goff, F.E., 1977. Vesicle cylinders in vapor-differentiated basalt flows. Ph.D. Thesis, Univ. California, Santa Cruz, CA.

Greenland, L.P., Rose, W.J. and Stokes, J.B., 1985. An estimate of gas emissions and magmatic gas content from Kilauea volcano. Geochim. Cosmochim. Acta, 49: 125–129.

Head, J.W. and Wilson, L., 1987. Lava fountain heights at Pu'u 'O'o, Kilauea, Hawaii: Indicators of amount and variations of exsolved magma volatiles. J. Geophys. Res., 92: 13,715–13,719.

Herd, R.A. and Pinkerton, H., 1993. Bubble coalescence in magmas. Lunar Planet. Science Congress, XXIV: 641–642 (abstract).

Jacobs, G.K., Spalding, B.P., Carter, J.G. and Koegler, S.S., 1988. In Situ Vitrification demonstration for the stabilization of buried wastes at the Oak Ridge National Laboratory. Nucl. Chem. Waste Manage., 8: 249–259.

Jaupart, C. and Vergniolle, S., 1988. Laboratory models of Hawaiian and Strombolian eruptions. Nature, 331: 58–60.

Jaupart, C. and Vergniolle, S., 1990. The generation and collapse of a foam foyer at the roof of a basaltic magma chamber. J. Fluid Mech., 203: 347–380.

Khitarov, N.I., Lebedev, Ye.B., Dorfman, A.M. and Bagdasarov, N. Sh., 1979. Effects of temperature, pressure, and volatiles on the surface tension of motten basalt. Geochem. Int., 16: 78–86.

Koch, D.L. and Shaqfeh, E.S.G., 1989. The instability of a dispersion of sedimenting spheroids. J. Fluid Mech., 209: 521–542.

Manga, M. and Stone, H.A., 1993. Buoyancy-driven interactions between deformable drops at low Reynolds numbers. J. Fluid Mech., 256: 647–683.

Mangan, M.T., Cashman, K.V. and Newman, S., 1993. Vesiculation of basaltic magma during eruption. Geology, 21: 157–160.

McMillan, K., Cross, R.W. and Long, P.E., 1987. Two-stage vesiculation in the Cohasett flow of the Grande Ronde Basalt, South-central Washington. Geology, 15: 809–812.

Philpotts, A.R. and Lewis, C.L., 1987. Pipe vesicles—An alternate model for their origin. Geology, 15: 971–974.

Proussevitch, A.A., Sahagian, D.L. and Anderson, A.T., 1993a. Dynamics of diffusive bubble growth in magmas: Isothermal case. J. Geophys. Res., 98: 22,283–22,307.

Proussevitch, A.A., Sahagian, D.L. and Kutolin, V.A., 1993b. Stability of foams in silicate melts. J. Volcanol. Geotherm. Res., 59: 161–178.

Ripepe, M., Rossi, M. and Saccorotti, G., 1993. Image processing of explosive activity at Stromboli. J. Volcanol. Geotherm. Res., 54: 335–351.

Sahagian, D.L., 1985. Bubble migration and coalescence during the solidification of basaltic lava flows. J. Geol., 93: 205–211.

Sahagian, D.L., Anderson, A.T. and Ward, B., 1989. Bubble coalescence in basalt flows: Comparison of a numerical

model with natural examples. Bull. Volcanol., 52: 49–56.
Sarda, S. and Graham, D., 1990. Mid-ocean ridge popping rocks: Implications for degassing at ridge crests. Earth Planet. Sci. Lett., 97: 268–289.
Schwindinger, K.R. and Anderson, A.T., 1989. Synthesis of Kilauea Iki olivines. Contrib. Mineral. Petrol., 103: 187–198.
Sparks, R.S.J., 1978. The dynamics of bubble formation in magmas: A review and analysis. J. Volcanol. Geotherm. Res., 3: 1–37.
Toramoru, A., 1988. Formation of propagation pattern in two-phase flow systems with application to volcanic eruptions. Geophys. J., 95: 613–623.
Toramoru, A., 1990. Measurement of bubble size distributions in vesiculated rocks with implications for quantitative estimate of eruption processes. J. Volcanol. Geotherm. Res., 43: 71–90.
Vergniolle, S. and Jaupart, C., 1986. Separated two-phase flow and basaltic eruptions. J. Geophys. Res., 91: 12,842–12,860.
Vergniolle, S. and Jaupart, C., 1990. Dynamics of degassing at Kilauea Volcano, Hawaii. J. Geophys. Res., 95: 2793–2809.
Walker, G.P.L., 1987. Pipe vesicles in Hawaiian basaltic lava: Their origin and potential as paleoslope indicators. Geology, 15: 84–87.
Walker, G.P.L., 1989. Spongy pahoehoe in Hawaii: A study of vesicle-distribution patterns in basalt and their significance. Bull. Volcanol., 51: 199–209.
Walker, D. and Mullins Jr., O., 1981. Surface tension of natural silicate melts from 1200°–1500° and implications for melt structure. Contrib. Mineral. Petrol., 76: 455–462.
Wilson, L. and Head, J.W., 1981. Ascent and eruption of basaltic magma on the Earth and Moon. J. Geophys. Res., 86: 2971–3001.
Zhang, X. and Davis, R.H., 1991. The rate of collisions due to Brownian motion of gravitational motion of small drops. J. Fluid Mech., 230: 479–504.